Miner Petrol (2013) 107:665–677
DOI 10.1007/s00710-012-0205-y

SPECIAL ISSUE GONDWANA COLLISION

$^{40}Ar/^{39}Ar$ record of late Pan–African exhumation of a granulite facies terrain, central Dronning Maud Land, East Antarctica

Bart W. H. Hendriks · Ane K. Engvik · Synnøve Elvevold

Received: 21 September 2011 / Accepted: 17 May 2012 / Published online: 8 June 2012

Abstract $^{40}Ar/^{39}Ar$ geochronological data on hornblende, biotite and K-feldspar provide constraints on the cooling path experienced by a high-grade metamorphic complex from the Mühlig–Hofmannfjella and Filchnerfjella (6–8°E), central Dronning Maud Land, Antarctica, during the late Neoproterozoic-early Palaeozoic Pan–African orogeny. Hornblende ages yield c. 481 Ma, biotite ages range from c. 466 Ma to c. 435 Ma, whereas K-feldspar ages of the gneisses are c. 437 Ma. The $^{40}Ar/^{39}Ar$ data suggest initial cooling at a rate of ~10 °C/Myr between 481 and 465 Ma, followed by a lower cooling rate of ~6 °C/Myr during the subsequent c. 30 million years. The K-feldspar $^{40}Ar/^{39}Ar$ ages place a lower time limit on the duration of the exhumation, by the time of thermal relaxation to a stable continental geotherm. The $^{40}Ar/^{39}Ar$ data reflecting cooling indicate tectonic exhumation related to orogenic collapse during a later phase of the Pan–African orogeny.

Editorial handling: M. Brown

Electronic supplementary material The online version of this article (doi:10.1007/s00710-012-0205-y) contains supplementary material, which is available to authorized users.

B. W. H. Hendriks (✉) · A. K. Engvik
Geological Survey of Norway,
7491 Trondheim, Norway
e-mail: bart.hendriks@ngu.no

A. K. Engvik
e-mail: ane.engvik@ngu.no

S. Elvevold
Norwegian Polar Institute,
9296 Tromsø, Norway
e-mail: Elvevold@npolar.no

Introduction

Geochronological studies within Dronning Maud Land (DML), Antarctica, have revealed that the crust formed at c. 1.1–1.0 Ga during the Mesoproterozoic, and was metamorphosed and intruded by voluminous magmatic bodies in the late Neoproterozoic-early Palaeozoic (Ohta et al. 1990; Moyes 1993; Mikhalsky et al. 1997; Jacobs et al. 1998; Paulsson and Austrheim 2003). The late Neoproterozoic-early Palaeozoic activity was related to the Pan–African orogeny and assembly of Gondwana forming the East–African–Antarctic orogen (e.g. Stern 1994; Meert 2003; Jacobs and Thomas 2004). The East–African–Antarctic orogen is up to 1,000 km wide and extends for more than 8,000 km along the eastern margin of Africa and into East Antarctica, and resulted from multiplate collision of various parts of East– and West–Gondwana.

Pan–African granulite-facies metamorphism is frequently reported from areas that were involved in the Gondwana assembly (e.g. Harley 2003). Within central DML, granulite facies metamorphism, dated at 625–515 Ma (Mikhalsky et al. 1997; Jacobs et al. 1998; Henjes-Kunst 2004), reached 800–900 °C (Bucher-Nurminen and Ohta 1993; Bisnath and Frimmel 2005; Piazolo and Markl 1999; Colombo and Talarico 2004; Elvevold and Engvik 2012). Structural studies in combination with geochronology and petrology have revealed an early compressional event followed by a later extensional phase (Jacobs et al. 2003a; Bauer et al. 2004). The later phase of the Pan–African event in central DML is characterised by a decompressional P–T history and extensional structures which indicate tectonic exhumation (Jacobs et al. 2003b; Engvik and Elvevold 2004). Based on the tectonometamorphic evolution of the Pan–African orogeny of Filchnerfjella (Fig. 1; Engvik and Elvevold 2004), $^{40}Ar/^{39}Ar$ geochronology is used to constrain the timing of the cooling history during unroofing. The results are discussed in the broader context of the early Palaeozoic evolution of East Antarctica. Application of $^{40}Ar/^{39}Ar$-geochronology to hornblende, biotite and K-feldspar reveals a cooling history with ages representing temperatures from 550 to 650 °C down to c. 200–250 °C (Harrison 1981; Harrison and McDougall 1982; Villa and Puxeddu 1994; Villa 1998; McDougall and Harrison 1999; Allaz et al. 2011). The data are further used to deduce cooling rates for this part of the orogen.

Geological setting and tectonometamorphic evolution

Central DML consists of a series of granitoid intrusive rocks, which are emplaced in granulite– and upper amphibolite facies metamorphic country rocks (e.g. Bucher-Nurminen and Ohta 1993; Piazolo and Markl 1999; Engvik and Elvevold 2004; Roland 2004; Bucher and Frost 2005; D'Souza et al. 2006). The igneous suite extends from 6 to 13°E and comprises charnockite, syenite, quartz syenite, granite and several generations of dykes ranging in composition from granitic to gabbroic/dioritic.

The nunataks of Mühlig–Hofmannfjella and Filchnerfjella (6–8°E) consist of banded gneiss, migmatites, and younger post-kinematic quartz syenite (Figs. 1 and 2). The metamorphic sequence includes metapelites, and leucocratic, intermediate and mafic igneous rocks (Elvevold and Engvik 2012). The different rock types form layers, which vary in thickness from <1 m up to several tens of meters. The granulite facies

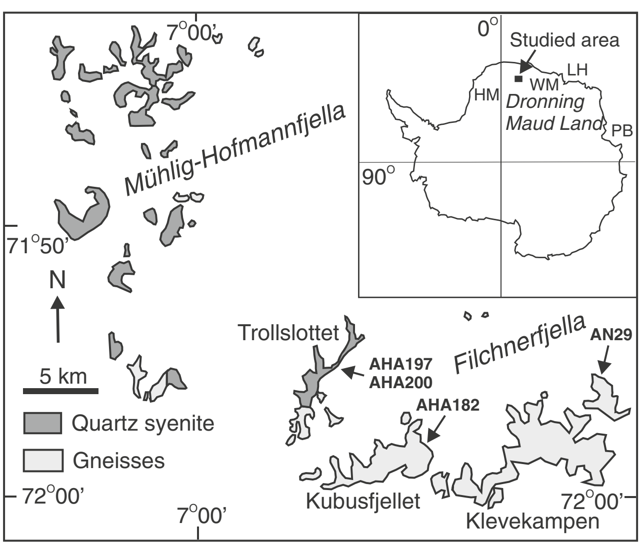

Fig. 1 Geological map of eastern Mühlig–Hofmann– and Filchnerfjella, central Dronning Maud Land, Antarctica. Sample locations are shown. HM = Heimefrontfjella, WM = Wohlthatmassiv, LH = Lützow Holmbukta, PB = Prydz Bay

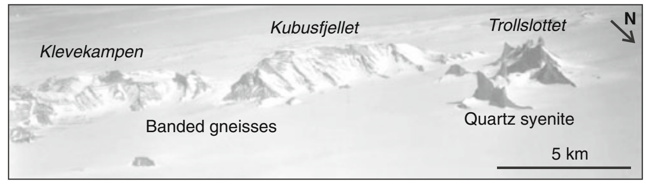

Fig. 2 Oblique aerial photograph of Filchnerfjella showing the banded gneisses exposed in Klevekampen and Kubusfjellet, and the intrusive quartz syenite in Trollslottet. (Photo: Norwegian Polar Institute)

metamorphism in central DML is dated by $^{207}Pb/^{206}Pb$ and U-Pb on zircons to between 625 and 515 Ma (Mikhalsky et al. 1997; Jacobs et al. 1998; Henjes-Kunst 2004). The quartz syenite is a part of the igneous suite intruding the banded gneisses. The syenites of central DML are dated by U-Pb on zircons to between 540 and 510 Ma (Mikhalsky et al. 1997; Paulsson 2003; Markl and Henjes-Kunst 2004).

The banded gneisses (Figs. 2 and 3a) typically comprise granulite facies mineralogy (Elvevold and Engvik 2012). Metapelitic rocks occur as garnet–biotite– and sillimanite–bearing gneisses and migmatites. Mafic and intermediate rocks contain orthopyroxene, amphibole, biotite, garnet and clinopyroxene in variable amounts. The banded gneisses experienced peak metamorphic conditions of about 800–900 °C at intermediate pressures of 0.5–1 GPa and migmatisation has affected large parts of the metamorphic sequence. Breakdown of Grt-Sill-Spl-bearing assemblages to Crd-bearing assemblages indicate that peak conditions were followed by near-isothermal decompression. The dominant E–W fabric illustrates transposition of migmatitic and leucocratic melts during the near-isothermal decompression. Extensional shear bands and shear zones evolved from the ductile partial melting stage through semiductile towards brittle conditions. Their occurrence shows that exhumation persisted towards brittle crustal conditions during tectonic W/SW-vergent extension (Engvik and Elvevold 2004). The quartz syenite (Figs. 2 and 3b) post-dates formation of the main fabric in the metamorphic sequence. The quartz syenite is mostly coarse-grained and contains megacrysts of mesoperthitic K-feldspar, with minor quartz, plagioclase and mafic minerals. The intrusion contains narrow semiductile to brittle shear zones, which suggest that the tectonic exhumation continued after their emplacement. A regional late-magmatic fluid infiltration event locally occurred along pegmatitic veins and is the last record of the Pan–African event affecting the area (Fig. 3c; Engvik et al. 2005; Engvik and Stöckhert 2007).

$^{40}Ar/^{39}Ar$ geochronology

$^{40}Ar/^{39}Ar$ analyses of mineral separates from selected samples were carried out at the Geological Survey of Norway.

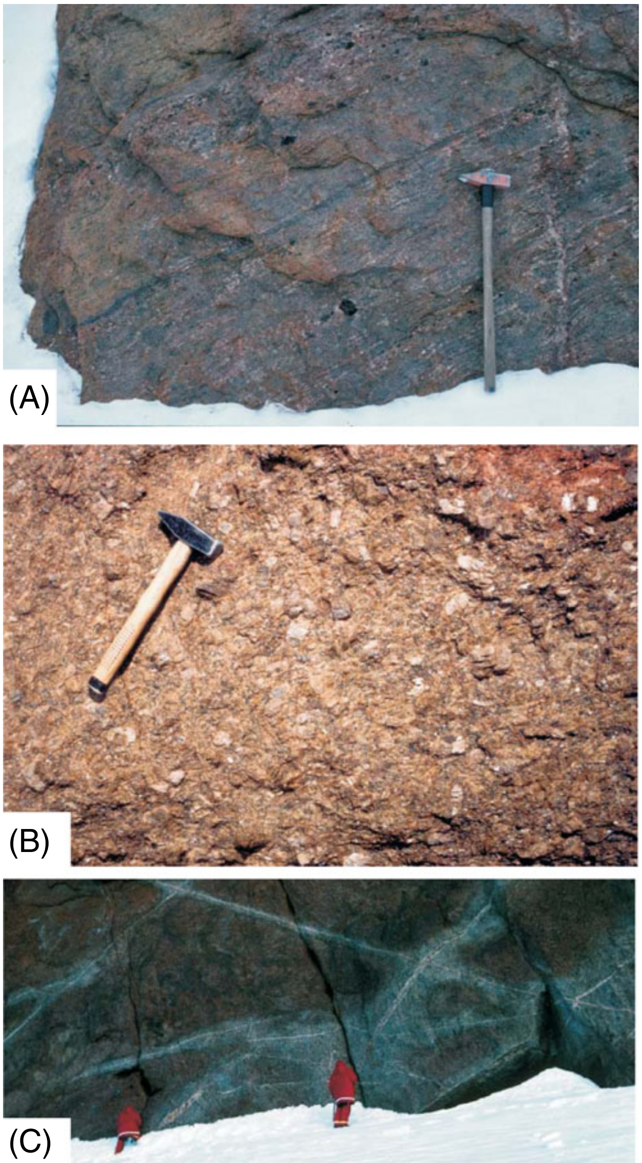

Fig. 3 Field pictures of **a**) Granulite facies migmatitic gneiss, Klevekampen, Filchnerfjella. **b**) Quartz syenite, Mühlig–Hofmannfjella. **c**) Fluid infiltration zones constituted by alteration halos along pegmatitic veins, Trollslottet. The alteration causes bleaching of the dark rock due to hydration mineral reactions and a high density of microcracks in feldspar and quartz

Mineral separates of K-feldspar, biotite and hornblende were analyzed by step-heating in a resistance furnace (AN29 and AHA182) or with a CO_2 laser (AHA197 and AHA200). Detailed analytical procedures are presented in the Electronic supplement. An overview of the results is presented in Table 1 and complete data tables are reported in the Electronic supplement. The $^{40}Ar/^{36}Ar$ intercept ratios calculated from the inverse isochrons (Table 1) overlap the atmospheric value of 298.56±0.31 (Lee et al. 2006) within 2σ in all cases, except for AHA200 Hornblende (for which the inverse isochron in any case has an unacceptably high MSWD). In our discussion of the age results we rely on the plateau ages.

Four samples were selected for analyses, each sample contains hornblende, biotite, and K-feldspar in the paragenesis. Mineral chemical data for the dated phases are presented in Table 2. The quantitative microanalyses were performed using a Cameca SX100 electron microprobe equipped with 5 wave length-dispersive spectrometers (WDS) at the Institute of Geosciences, University of Oslo. The accelerating voltage was 15 kV and the counting time 10 s on peak using a beam current of 15 nA. A defocused beam (10 m) was used for K-feldspar. Standardization was made on a selection of synthetic and natural minerals and oxides. Data reduction was done by the PAP program (Pouchou and Pichoir 1984). Sample locations are shown in Fig. 1.

Sample descriptions

Samples AN29 and AHA182 were collected from migmatite at Klevekampen and Kubusfjellet, respectively. The orthopyroxene-bearing migmatite is heterogranular, fine– to medium–grained. Its characteristic dark brown colour is typical for the granulite facies rocks in the area. Anhedral quartz, plagioclase and K-feldspar grains, 0.5–2 mm in diameter, are predominant. K-feldspars ($Or_{85-91}Ab_{9-15}$) are present as microperthite. Hornblende (Mg/(Mg + Fe)=0.19–0.23; K=0.33–0.36 p.f.u.; Ca=1.86–1.87; Cl=0.03–0.04) and biotite (Mg/(Mg + Fe)=0.26–0.28; Cl=0.03–0.04) are concentrated in thin layers together with orthopyroxene (Fig. 4a). Amphibole shows no zoning except for a small rimward lowering in Na up to 0.08 p.f.u. Ilmenite, apatite, monazite and zircon are present as accessory minerals.

Samples AHA197 and AHA200 were collected at Trollslottet. The quartz syenite, which makes up Trollslottet nunatak, is dominated by microperthitic K-feldspar ($Or_{83-84}Ab_{16-17}$), quartz and plagioclase. The microtexture is strongly heterogranular, with microperthite as subhedral laths up to 5 cm, set in a medium grained matrix of quartz, plagioclase and mafic minerals. Myrmekite is common. 5–10 % mafic minerals are present, mostly as hornblende (Mg/(Mg + Fe)=0.33; K=0.28 p.f.u.; Ca=1.90; Cl=0.03) and biotite (Mg/(Mg + Fe)=0.34; Cl=0.04) (Fig. 4b). Orthopyroxene is replaced by fine-grained iddingsite, or often altered to grunerite. Apatite, ilmenite, zircon, allanite and hematite are accessory minerals. Minor and local alteration of microperthite is observed along micro fractures. Sample AHA200, which is sampled 1.5 m away from sample AHA197, is strongly altered due to late-magmatic fluid infiltration. K-feldspar of the altered quartz syenite is $Or_{89}Ab_{12}$ and shows replacement to microcline. AHA200 also is the only sample where sericite and chlorite are

Table 1 Summary table of $^{40}Ar/^{39}Ar$-data. 'Steps used' refers to the step numbers used in the age calculation. $\%^{39}Ar$ = the percentage of cumulative ^{39}Ar gas represented by the indicated steps. $^{40}Ar/^{36}Ar$ is the intercept on the vertical of the inverse isochron diagram. MSWD, mean square weighted deviation. Prob., probability of fit e.g. Chidist(MSWD*df,df). T/OP, Temperature (oven samples) or Operating Power (CO_2 laser). TFA = total fusion age. All uncertainties reported at 2σ

Sample	Mineral	Steps used T/OP	cum39Ar (%)	Spectrum age	2 s	MSWD	Prob.	Isochron age	2 s	MSWD	Prob.	$^{40}Ar/^{36}Ar$	2 s	TFA	2 s
AHA197	K-feldspar	4 to 14 (−8)	81.23	432.33	6.20	9.29	0.00	435.76	9.82	9.91	0.00	219.10	122.41	428.03	3.59
		4.0–7.5 (−4.8)	Weighted mean												
	Biotite	3 to 8	77.00	451.75	4.69	1.77	0.12	448.38	6.06	1.35	0.25	346.87	61.73	450.21	3.89
		3.4–4.7		Plateau											
	Hornblende	5 to 12	87.81	484.89	8.54	10.09	0.00	489.78	13.36	10.94	0.00	255.90	93.56	521.34	4.66
		4.0–6.3		Weighted mean											
		6 to 9	44.25	477.65	6.46	2.29	0.08	475.93	9.78	2.97	0.05	317.21	68.92	521.34	4.66
		4.2–5.0		Weighted mean											
AHA200	K-feldspar	4 to 12	48.84	432.50	4.64	2.09	0.03	434.92	6.01	2.04	0.05	260.43	62.51	430.69	4.01
		3.5–6.8		Weighted mean											
	Biotite	2 to 9	71.43	434.92	3.88	0.80	0.59	435.58	4.36	0.87	0.51	287.41	37.63	427.03	3.86
		3.0–4.9		Plateau											
	Hornblende	5 to 14	89.10	461.93	9.22	14.65	0.00	470.71	20.62	14.52	0.00	177.91	113.83	487.04	4.26
		3.9–8.0		Weighted mean								No overlap with atmospheric $^{40}Ar/^{36}Ar$			
AN29	K-feldspar	5 to 14	92.17	423.93	7.21	18.71	0.00	426.06	7.97	19.61	0.00	281.64	36.76	431.94	3.49
		595–1,023 C		Weighted mean											
	Biotite	1 to 10	98.98	464.48	3.76	1.13	0.34	464.83	3.77	1.12	0.35	292.17	11.52	463.58	4.03
		409–1,132 C		Plateau											
	Hornblende	8 to 11	85.07	481.14	5.62	0.29	0.84	482.19	6.23	0.21	0.81	267.97	81.77	490.19	7.57
		979–1,219 C		Plateau											
AHA182	K-feldspar	8 to 13	68.35	436.90	3.39	0.68	0.64	436.88	3.57	0.85	0.49	303.63	131.71	428.05	3.69
		885–1,308 C		Plateau											
	Biotite	4 to 15	96.53	465.80	3.66	0.41	0.95	465.88	3.72	0.45	0.92	297.90	7.45	468.84	3.93
		595–1,121 C		Plateau											
	Hornblende	5 to 10	86.06	492.22	6.93	6.09	0.00	495.84	10.43	2.29	0.06	250.715	54.320	508.72	8.60
		1,048–1,309 C		Weighted mean				1,151–1,309 C, 49.73 % cum. ^{39}Ar							

Table 2 Mineral chemical data of amphiboles, biotites and K-feldspar

Chemistry of amphiboles

Sample	AN29	AN29	AHA182	AHA182	AHA197	AHA200	AHA200
Analyse No.	3/1.	4/1.	18/1.	19/1.	5.4a	33/1.	34/1.
SiO_2	39.91	39.83	40.03	40.24	42.64	40.17	39.54
Al_2O_3	10.14	10.85	10.08	9.82	8.75	8.92	9.83
TiO_2	2.10	1.46	1.97	2.13	1.60	1.91	1.31
Cr_2O_3	0.03	0.04	0.04	0.09	0.08	0.01	0.00
FeO	26.78	27.16	26.39	26.12	23.27	26.63	26.66
MnO	0.23	0.25	0.24	0.20	0.24	0.61	0.59
MgO	4.06	3.54	4.35	4.44	6.41	4.20	4.04
CaO	10.88	11.02	10.88	10.91	11.31	10.99	11.25
Na_2O	1.73	1.50	1.67	1.58	1.47	1.80	1.72
K_2O	1.76	1.72	1.68	1.61	1.38	1.56	1.79
Cl	0.13	0.12	0.13	0.12	0.11	0.43	0.60
SUM	97.76	97.49	97.45	97.25	97.26	97.24	97.35
Cl = O	0.03	0.03	0.03	0.03	0.02	0.10	0.14
SUM	97.73	97.47	97.42	97.23	97.24	97.15	97.21
Comment	core	rim	core	rim	core	core	rim
Structural formula based on 23 O							
Si	6.37	6.38	6.39	6.43	6.68	6.48	6.40
Al	1.91	2.05	1.90	1.85	1.61	1.70	1.88
Ti	0.25	0.18	0.24	0.26	0.19	0.23	0.16
Cr	0.00	0.01	0.00	0.01	0.01	0.00	0.00
Fe	3.58	3.64	3.53	3.49	3.05	3.59	3.61
Mn	0.03	0.03	0.03	0.03	0.03	0.08	0.08
Mg	0.97	0.85	1.04	1.06	1.50	1.01	0.97
Ca	1.86	1.89	1.86	1.87	1.90	1.90	1.95
Na	0.54	0.47	0.52	0.49	0.45	0.56	0.54
K	0.36	0.35	0.34	0.33	0.28	0.32	0.37
Cl	0.04	0.03	0.03	0.03	0.03	0.12	0.17
SUM cat	15.87	15.83	15.85	15.80	15.68	15.88	15.96
Ca/K ratio	5.19	5.38	5.44	5.69	6.88	5.93	5.27
Cl/K ratio	0.10	0.09	0.10	0.10	0.11	0.37	0.45
Mg/(Mg + Fe)	0.21	0.19	0.23	0.23	0.33	0.22	0.21

Chemistry of biotites

Sample	AN29	AN29	AHA182	AHA182	AHA197	AHA200	AHA200
Analyse No.	6/1.	7/1.	21/1.	22/1.	5.9	30/1.	31/1.
SiO_2	34.56	35.08	34.63	35.12	34.91	35.58	35.15
Al_2O_3	12.55	12.50	12.59	12.71	12.52	12.56	12.58
TiO_2	4.97	4.74	5.05	5.01	4.25	3.02	3.47
Cr_2O_3	0.02	0.04	0.00	0.05	0.12	0.02	0.00
FeO	28.10	28.33	27.48	27.58	25.88	28.12	27.75
MnO	0.11	0.13	0.07	0.07	0.02	0.38	0.40
MgO	5.62	5.68	5.88	5.99	7.50	6.57	6.26
CaO	0.02	0.00	0.00	0.00	0.02	0.00	0.00
Na_2O	0.08	0.08	0.07	0.10	0.10	0.05	0.05
K_2O	9.52	9.74	9.68	9.67	8.98	9.49	9.38

Table 2 (continued)

Chemistry of amphiboles							
Sample	AN29	AN29	AHA182	AHA182	AHA197	AHA200	AHA200
Cl	0.13	0.13	0.11	0.11	0.14	0.52	0.49
SUM	95.68	96.42	95.53	96.35	94.44	96.27	95.49
Cl = O	0.03	0.03	0.03	0.02	0.03	0.12	0.11
SUM	95.65	96.40	95.51	96.32	94.41	96.16	95.38
Structural formula based on 22 O							
Si	5.55	5.59	5.56	5.58	5.60	5.69	5.66
Al	2.38	2.35	2.38	2.38	2.37	2.37	2.39
Ti	0.60	0.57	0.61	0.60	0.51	0.36	0.42
Cr	0.00	0.00	0.00	0.01	0.02	0.00	0.00
Fe	3.77	3.78	3.69	3.66	3.47	3.76	3.74
Mn	0.01	0.02	0.01	0.01	0.00	0.05	0.05
Mg	1.34	1.35	1.41	1.42	1.79	1.57	1.50
Ca	0.00	0.00	0.00	0.00	0.00	0.00	0.00
Na	0.02	0.02	0.02	0.03	0.03	0.02	0.02
K	1.95	1.98	1.98	1.96	1.84	1.94	1.93
Cl	0.04	0.03	0.03	0.03	0.04	0.14	0.13
SUM kat	15.64	15.66	15.65	15.63	15.63	15.74	15.70
Ca/K ratio	0.00	0.00	0.00	0.00	0.00	0.00	0.00
Cl/K ratio	0.02	0.02	0.02	0.01	0.02	0.07	0.07
Mg/(Mg + Fe)	0.26	0.26	0.28	0.28	0.34	0.29	0.29

Chemistry of K-feldspar							
Sample	AN29	AN29	AHA182	AHA182	AHA197	AHA197	AHA200
Analyse No.	9/1.	15/1.	26/1.	29/1.	5.2b	5.5b	
Na_2O	1.26	1.51	1.05	1.68	1.84	1.82	1.31
K_2O	15.13	15.06	15.90	14.80	14.38	13.84	15.24
SiO_2	64.75	64.65	64.13	64.47	64.52	64.54	64.58
Al_2O_3	18.34	18.52	18.33	18.57	17.81	18.19	18.35
CaO	0.01	0.01	0.02	0.10	0.04	0.03	0.00
FeO	0.01	0.05	0.00	0.02	0.00	0.01	0.04
BaO	0.40	0.43	0.44	0.33	0.52	0.43	0.49
sum	99.90	100.22	99.87	99.97	99.11	98.86	99.94
Comment	homogenous	fine erthite	homogenous	fine perthite	fine perthite	fine perthite	fine perthite average 8 points
Structural formula based on 5 cations							
Si	2.99	2.97	2.96	2.96	3.00	3.01	2.98
Al	1.00	1.00	1.00	1.01	0.97	1.00	1.00
Fe	0.00	0.00	0.00	0.00	0.00	0.00	0.00
Ca	0.00	0.00	0.00	0.00	0.00	0.00	0.00
Ba	0.01	0.01	0.01	0.01	0.01	0.01	0.01
Na	0.11	0.13	0.09	0.15	0.17	0.16	0.12
K	0.89	0.88	0.94	0.87	0.85	0.82	0.90
Ca/K ratio	0.00	0.00	0.00	0.01	0.00	0.00	0.00
Or	88.8	86.7	90.8	84.9	83.6	83.2	88.7
Ab	11.2	13.2	9.1	14.6	16.2	16.6	11.6

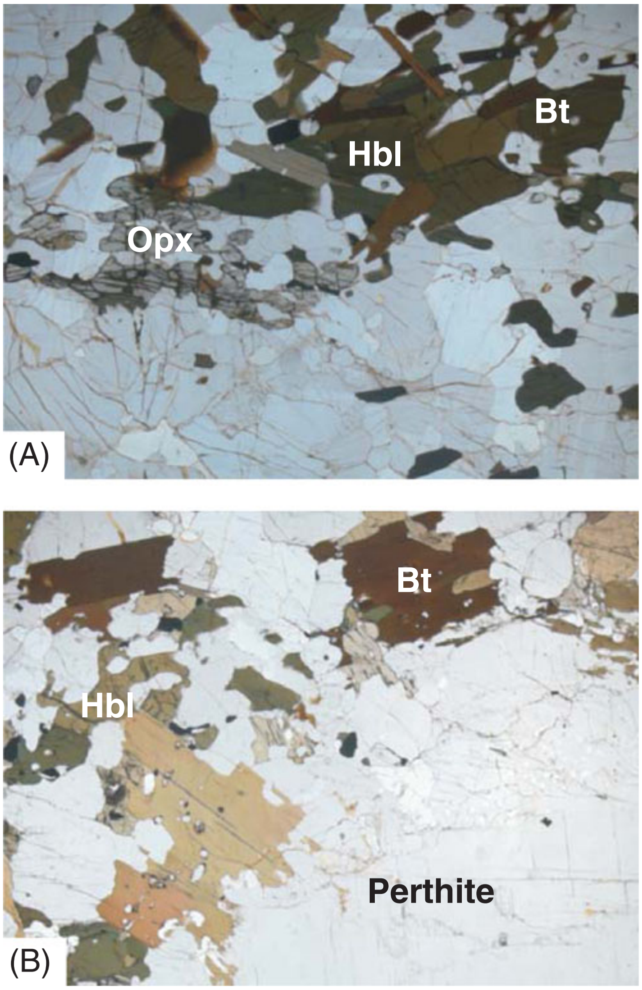

Fig. 4 Photomicrographs (abbreviations after Whitney and Evans 2010). **a**) Crystals of biotite and hornblende in Opx–bearing migmatitic gneiss. Sample AN29, width of image 5.3 mm. **b**) Hornblende and biotite crystals in quartz syenites. Part of microperthite lath is showed in lower right corner. Sample AHA197, width of image 5.3 mm

observed in thin section in feldspar and biotite respectively. Orthopyroxene and grunerite are absent, while biotite and hornblende have recrystallized into fine grained aggregates. Biotite is lower in Mg/(Mg + Fe), with a ratio of 0.29, and higher in Cl (0.13–0.14 p.f.u.) compared to biotite in the brown quartz syenite. The hornblende has Mg/(Mg + Fe)= 0.21–0.22, and a small rimward increase of Ca to 1.95 p.f.u. and K to 0.37 p.f.u., and a Cl-content of up to 0.17 p.f.u.

Hornblende age data

Age spectra and inverse isochron plots for hornblende separates are displayed in Fig. 5. Hornblende separated from sample AN29 yielded a statistically valid plateau age (481.14±5.62 Ma at 2σ; probability-of-fit 0.84) for 85.07 % of the cumulative ^{39}Ar. The three other hornblende spectra indicate perturbation of the K/Ar system. Not surprisingly this is most apparent for the strongly altered sample, AHA200. The Cl/K ratio for this sample is higher than for the other hornblende separates, as confirmed by mineral chemical data (Table 2; Cl/K=0.4 for both rim and core). No systematic variation of step ages with Ca/K or Cl/K ratio is apparent however for hornblende samples AHA182, AHA197 or AHA200. Inverse isochron ages for AHA197 hornblende (475.93±9.78 Ma at 2σ) and AHA182 Hornblende (495.84±10.43 Ma at 2σ) have probability-of-fit values at the minimally acceptable value (0.05). However, this is for portions of the spectra (44.25 % and 49.73 % of the cumulative ^{39}Ar, respectively) that are too small for them to be considered robust ages. Despite their more complex spectra, the weighted mean ages for parts of the hornblende spectra for samples AHA182 and AHA197 indicate they likely recorded a similar event as AN29 hornblende (Fig. 5).

Biotite age data

Age spectra and inverse isochron plots for biotite separates are plotted in Fig. 6. All four samples analyzed yielded stable spectra, with statistically valid plateaus and inverse isochrons with $^{40}Ar/^{36}Ar$ ratio overlapping the atmospheric value for each sample. The biotite plateau ages for samples AN29 and AHA182 are virtually identical at 464.48± 3.76 Ma (2σ; probability-of-fit 0.34) and 465.80±3.66 Ma (2σ; probability-of-fit 0.95) respectively. For sample AHA197 the plateau age is younger by about 14 Ma at 451.75±4.69 Ma (2σ; probability-of-fit 0.12), with sample AHA200 yielding the youngest age of 434.92±3.88 Ma (2σ; probability-of-fit 0.59). As for AHA200 Hornblende, chemical data (Table 2) indicate a higher Cl/K ratio for AHA200 biotite compared to the other three biotite separates, again confirming the strongly altered nature of this sample.

K-feldspar age data

Age spectra and inverse isochron plots for K-feldspar samples are plotted in Fig. 7. For sample AHA182 a statistically valid plateau (436.90±3.39 Ma at 2σ; probability of fit 0.64) was obtained for 68.35 % of the cumulative ^{39}Ar. K-feldspar spectra for samples AHA197 and AHA200 indicate perturbed systems for which no statistically valid plateau or isochron ages can be calculated. Nevertheless, weighted mean ages for large parts of these two spectra overlap with the K-feldspar age for sample AHA182. Samples AHA182 and AN29 had nearly identical biotite ages, but as for AHA197 and AHA200 the AN29 K-feldspar the spectrum is disturbed. Figure 7a displays the age spectrum for AN29 K-feldspar together with the Ca/K ratio and the percentage of radiogenic ^{40}Ar. In the second part of the spectrum, from ~40 % cumulative ^{39}Ar and onwards, the percentage of radiogenic ^{40}Ar correlates positively with the step ages and negatively with the Ca/K content.

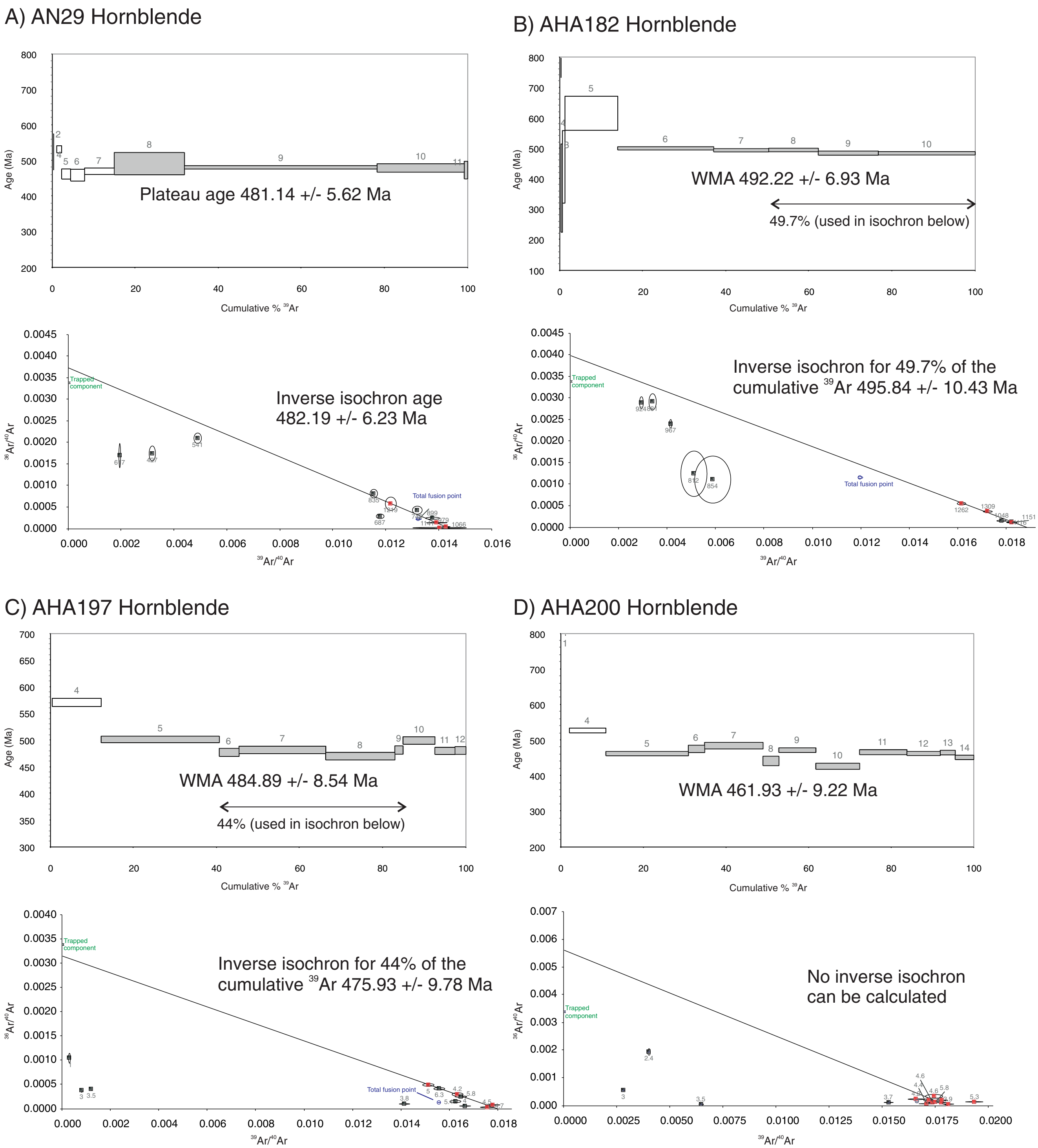

Fig. 5 $^{40}Ar/^{39}Ar$ release spectra (*top panels*) and inverse isochron diagrams (*bottom panels*) for hornblende separates. *Grey boxes* in the spectra represent steps included in the spectrum age calculation. *Red squares* in the inverse isochron diagrams represent steps included in the isochron calculation. WMA, weighted mean age. **a**) AN29. **b**) AHA182. **c**) AHA197. **d**) AHA200. All uncertainties and error envelopes at 2σ

This suggests that the disturbance of the AN29 K-feldspar spectrum may partly be compositionally controlled. The high temperature steps in the AN29 K-feldspar spectrum overlap in age with the statistically robust age for AHA182 K-feldspar.

The statistically valid plateau and isochron ages for AHA182 K-feldspar provide a well-constrained timing for closure of the K/Ar system in K-feldspar. Despite the noted disturbances, the K-feldspar spectra for two other samples (AHA197, AHA200) apparently recorded the same cooling event.

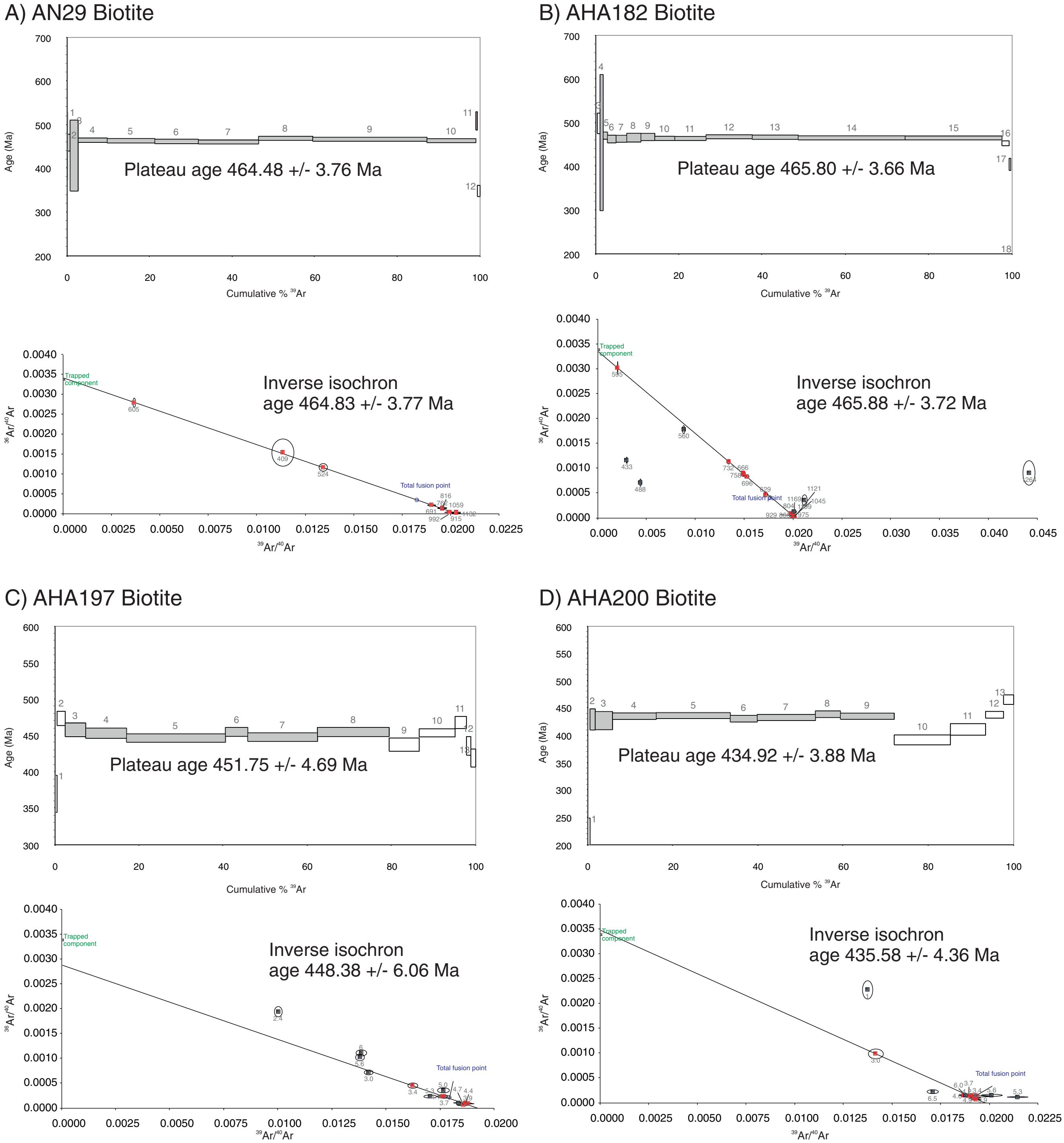

Fig. 6 $^{40}Ar/^{39}Ar$ release spectra (*top panels*) and inverse isochron diagrams (*bottom panels*) for biotite separates. *Grey boxes* in the spectra represent steps included in the spectrum age calculation. *Red squares* in the inverse isochron diagrams represent steps included in the isochron calculation. **a**) AN29. **b**) AHA182. **c**) AHA197. **d**) AHA200. All uncertainties and error envelopes at 2σ

Discussion

Cooling history

Robust $^{40}Ar/^{39}Ar$ plateau ages on hornblende (481.14±5.62 at 2σ), biotite (465.80±3.66 and 464.48±3.76 at 2σ) and K-feldspar (436.90±3.39 at 2σ) are available for migmatite from Filchnerfjella. For the fresh quartz syenite (AHA197), a robust biotite plateau age (451.75±4.69 at 2σ) and a disturbed K-feldspar spectrum that nevertheless is compatible with the K-feldspar age of the migmatite was obtained. The strongly altered quartz syenite has an even younger

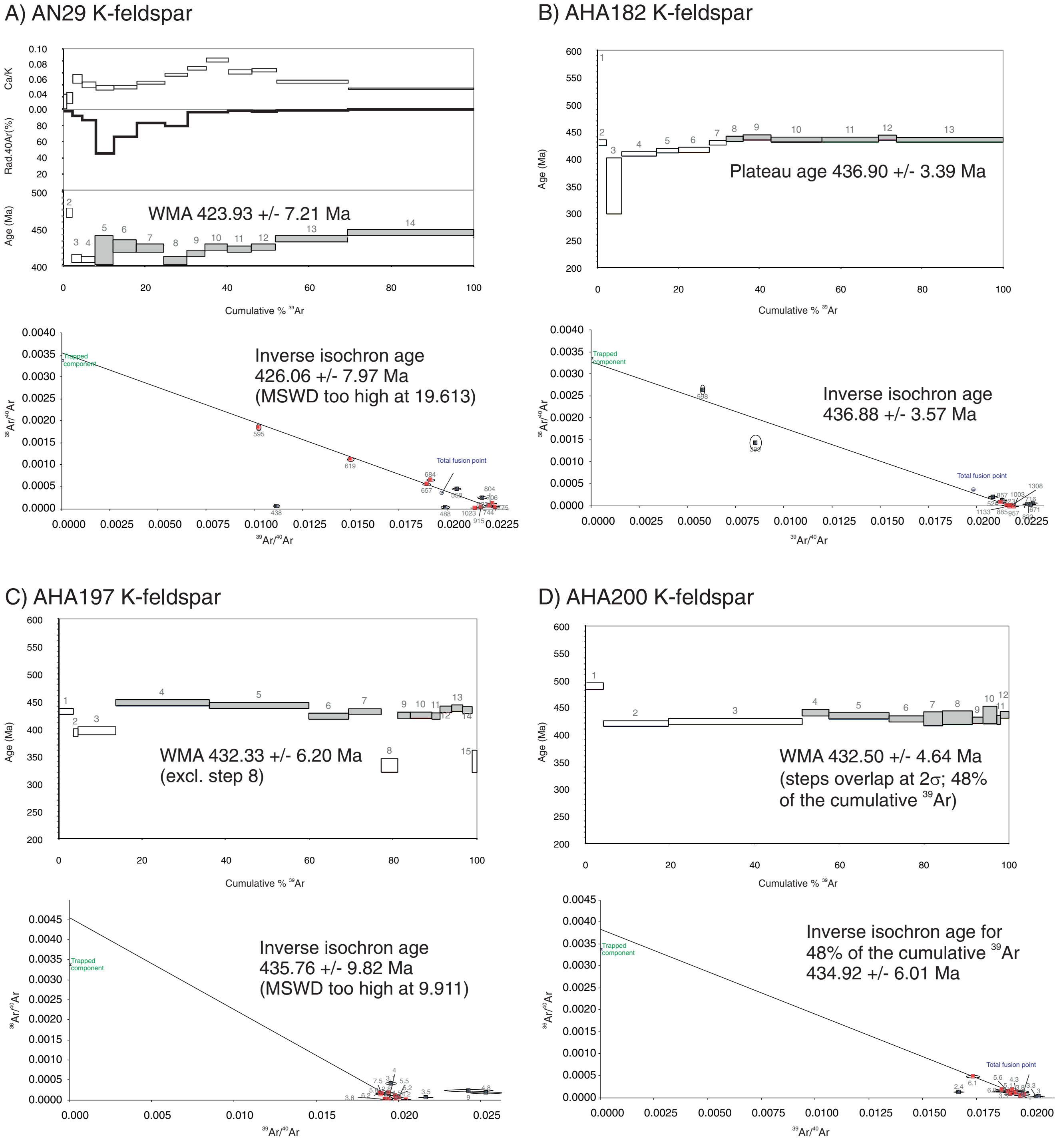

Fig. 7 $^{40}Ar/^{39}Ar$ release spectra (*top panels*) and inverse isochron diagrams (*bottom panels*) for K-feldspar separates. *Grey boxes* in the spectra represent steps included in the spectrum age calculation. *Red squares* in the inverse isochron diagrams represent steps included in the isochron calculation. WMA, weighted mean age. MSWD, mean square weighted deviation. **a**) AN29. **b**) AHA182. **c**) AHA197. **d**) AHA200. All uncertainties and error envelopes at 2σ

biotite age of 434.92±3.88 Ma (2σ), which overlaps with the robust K-feldspar age of the migmatite. The younger biotite ages of the quartz syenite can be explained by a slower/later cooling of the large intrusion than the host gneisses, while the crustal temperature distribution has equilibrated by the time reflected by K-feldspar ages. The altered quartz syenite sample (AHA200) was taken with only 1.5 m separation from the dark, fresh quartz syenite (sample AHA197). The relatively poor constraints on the hornblende age of the altered quartz syenite might be interpreted as an effect of the late-magmatic fluid infiltration, explaining the relatively high Cl/K ratio (Table 2) of this sample. The fluid infiltration caused local heating and partial replacement of the mineralogy of the host rock (Engvik et al. 2009). A similar effect of fluid infiltration on the age distribution is shown by Markl and Henjes-Kunst (2004).

The Pan–African granulite facies metamorphism in central DML is dated between 625 and 515 Ma, while the syenites and charnockites intruded between 540 and 510 Ma (Mikhalsky et al. 1997; Jacobs et al. 1998; Markl and Henjes-Kunst 2004; Henjes-Kunst 2004). The gneisses in Filchnerfjella experienced peak metamorphic conditions of 800–900 °C at intermediate pressures followed by near-isothermal decompression (Engvik and Elvevold 2004). This near-isothermal decompression was accompanied by extension and magmatic intrusions, followed by cooling. The magmatic activity was associated with a slightly raised (30–40 °C/km) geothermal gradient. The late– and post–Pan–African cooling ages reflects crustal levels about 0.2–0.4 GPa (Engvik et al. 2005). By that time, the crust had relaxed to a stable continental geotherm of ~20 °C/km.

The $^{40}Ar/^{39}Ar$-ages demonstrate that the cooling took place during the later stage of the Pan–African orogeny. The cooling history (Fig. 8) is based on estimates of 'closure-temperatures' from literature data. For hornblende, estimates are in the range of 500–550 °C (Harrison 1981) to 550–650 °C (Villa 1998), based on laboratory experiments

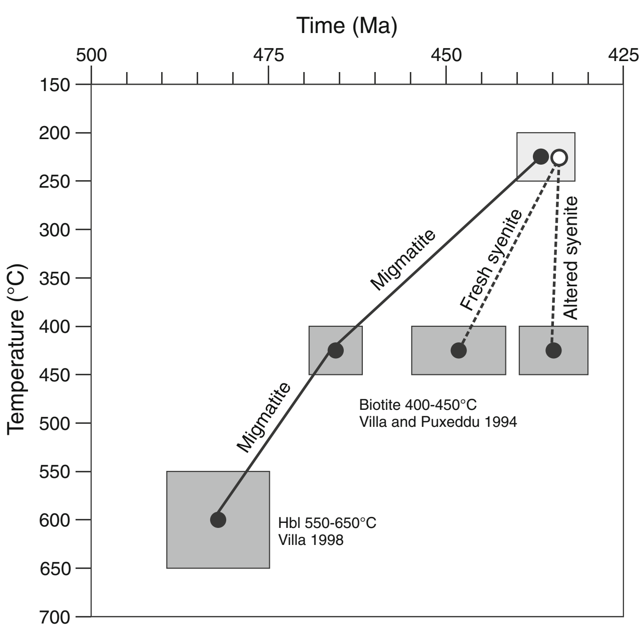

Fig. 8 Cooling histories based on literature values for the closure temperature of hornblende (Villa 1998), biotite (Villa and Puxeddu 1994) and K-feldspar (Harrison and McDougall 1982). Robust plateau ages (*solid dots*) constrain the cooling history of Filchnerfjella migmatite. In the absence of robust K-feldspar ages for fresh and altered syenite at Trollslottet the timing of K-feldspar closure is based on more qualitative information from perturbed spectra (see text for discussion)

and geological data, respectively. For biotite a commonly cited figure based on hydrothermal laboratory experiments is 300–350 °C (Grove and Harrison 1996). Validation of similar laboratory determinations against fluid inclusion thermometry on natural samples however suggests the laboratory based determinations could be too low by as much as ~100 °C (Villa and Puxeddu 1994), implying the geologically relevant biotite closure temperature is more likely 400–450 °C. A range of 200–250 °C has been reported for the closure temperature of K-feldspar (Harrison and McDougall 1982).

Post-dating intrusion of the syenites, our best constraint on the timing of cooling below 550–650 °C (hornblende) for the migmatite is 481.14±5.62 Ma (2σ). Subsequent cooling down to 400–450 °C is well-constrained by biotite ages of 464.48±3.76 Ma (2σ) and 465.80±3.66 Ma (2σ), indicating a cooling rate of ~10 °C/Myr. Cooling continued subsequently at rates of ~6 °C/Myr, with K-feldspar ages indicating temperatures of about 200–250 °C at 436.90±3.39 Ma (2σ). Cooling rates based on closure temperatures derived from laboratory data (Harrison 1981; Grove and Harrison 1996) would differ somewhat, being ~12 °C/Myr (hornblende to biotite) and ~4 ° C/Myr (biotite to K-feldspar), respectively.

Regional comparison within East Antarctica

The $^{40}Ar/^{39}Ar$ hornblende– and biotite ages obtained in this study are similar to $^{40}Ar/^{39}Ar$ ages reported by Markl and Henjes-Kunst (2004) from the Eastern Mühlig–Hofmannfjella (7°E, 71°40′S, central DML). The $^{40}Ar/^{39}Ar$ amphibole– and biotite–ages from charnockite are 487.0±2.4 and 466.6±2.2 Ma, respectively. In the Schirmacheroase (11°30′E, 70°45′S, central DML), Henjes-Kunst (2004) achieved older amphibole ages of 590–575 Ma and biotite ages of 525–520 Ma from metamorphosed sills. From Heimefrontfjella (western DML), Jacobs et al. (1995) retrieved two tectonothermal events. The first event showed ages below 1,000 Ma, while a later Pan–African event was recorded in K/Ar– and $^{40}Ar/^{39}Ar$–ages of biotite and muscovite to 533–476 Ma.

Late Neoproterozoic/early Palaeozoic high-grade metamorphism followed by exhumation and tectonic extension is reported over a wide area of East Antarctica. The Lützow–Holm Bay (e.g. Fraser et al. 2000) and Prydz Bay areas (e.g. Thost et al. 1994) have experienced an evolution very similar to the one revealed in DML. Fraser et al. (2000) achieved $^{40}Ar/^{39}Ar$ biotite and hornblende ages between 510 and 460 Ma in the Lützow–Holm Bay, following after Pan–African granulite facies metamorphism and near-isothermal decompression. Zhao et al. (1997) reported $^{40}Ar/^{39}Ar$ hornblende age of 514±2 Ma, biotite ages between 500 and 490 Ma and K-feldspar ages around 455 Ma in the Prydz Bay, and reported cooling rates of

9–3 °C/Myr. Although the $^{40}Ar/^{39}Ar$ –geochronology ages of the Filchnerfjella show slightly younger ages, the data reported throughout the wider area of East Antarctica reflects the late Pan-African cooling history and show that the East Antarctica occurred as a large homogenous crustal fragment in the early Palaezoic. The younger ages of Filchnerfjella can be explained by a slightly later cooling after the intrusions of the voluminous magmatic bodies in the area.

After the late Pan-African cooling, East Antarctica underwent a longer time of relaxation before Gondwana breakup. The Gondwana breakup is reflected in apatite-fission-track data showing ages between 250 and 100 Ma throughout East Antarctica from Heimefrontfjella in the west to Prydz Bay in the east (Jacobs et al. 1995; Zhao et al. 1997; Meier et al. 2004).

Conclusions

$^{40}Ar/^{39}Ar$ geochronological data combined with petrological evidence, constrain the timing of late-orogenic tectono-metamorphic evolution of the high-grade metamorphic complex from the Mühlig–Hofmann– and Filchnerfjella in central DML. $^{40}Ar/^{39}Ar$ hornblende–, biotite– and K-feldspar cooling ages range from c. 481 to 437 Ma, and reflect late–Pan–African cooling during extension and exhumation. The ages indicate a cooling rate of~10 °C/Myr between 481 and 465 Ma, followed by nearly 30 million years of cooling at~6 °C/Myr. $^{40}Ar/^{39}Ar$ geochronological data reflecting the late Pan–African cooling history, reported throughout East Antarctica, are consistent and indicate that East Antarctica existed as a large homogenous crustal fragment in the early Palaezoic.

Acknowledgments Samples for this study were collected during the Norwegian Antarctica Research Expedition 1996/1997, financed by the Norwegian Research Council and Norwegian Polar Institute. The $^{40}Ar/^{39}Ar$ analytical work was supported by the Geological Survey of Norway. We thank two anomymous reviewers for constructive comments that helped to improve our manuscript.

References

Allaz J, Engi M, Berger A, Villa IM (2011) The effects of retrograde reactions and of diffusion on $^{40}Ar/^{39}Ar$ ages of micas. J Petrol 52:691–716

Bauer W, Jacobs J, Paech H-J (2004) Structural evolution of the metamorphic basement of Central Dronning Maud Land, East Antarctica. Geologische Jahrbuch B96:325–364

Bisnath A, Frimmel HE (2005) Metamorphic evolution of the Maud Belt: P-T-t path for high-grade gneisses in Gjelsvikfjella Dronning Maud Land, East Antarctica. J Afr Earth Sci 43:505–524

Bucher K, Frost BR (2005) Fluid transfer in high-grade metamorphic terrains intruded by anorogenic granites: the Thor range, Antarctica. J Petrol 47:567–593

Bucher-Nurminen K, Ohta Y (1993) Granulites and garnet-cordierite gneisses from Dronning Maud Land, Antarctica. J Metamorph Geol 11:691–703

Colombo F, Talarico F (2004) Regional Metamorphism in the High-Grade Basement of Central Dronning Maud Land, East Antarctica. Geologische Jahrbuch B96:7–47

D'Souza MJ, Prasad AVK, Ravindra R (2006) Genesis of ferropotassic a-type granitoid of Mühlig-Hofmannfjella, Central Dronning Maud Land, East Antarctica. In: Fütterer DK, Damaske D, Kleinschmidt G, Miller H, Tessensohn F (eds) Antarctica: contributions to global earth sciences. Springer Verlag, Berlin, pp 45–54

Eide EA, Osmundsen PT, Meyer GB, Kendrick MA, Corfu F (2002) The Nesna Shear Zone north-central Norway: an $^{40}Ar/^{39}Ar$ record of Early Devonian – Early Carboniferous ductile extension and unroofing. Norwegian Journal of Geology 82:317–339

Elvevold S, Engvik AK (2012) Pan-African decompressional P-T path recorded by granulites from central Dronning Maud Land, Antarctica. Mineralogy and Petrology (in press)

Engvik AK, Elvevold S (2004) Pan-African extension and near-isothermal exhumation of a granulite facies terrain, Dronning Maud Land, Antarctica. Geol Mag 141:649–660

Engvik AK, Stöckhert B (2007) The inclusion record of fluid evolution crack healing and trapping from a heterogenous system during rapid cooling of pegmatitic veins (Dronning Maud Land; Antarctica). Geofluids 7:171–185

Engvik AK, Kalthoff J, Bertram A, Stöckhert B, Austrheim H, Elvevold S (2005) Magma-driven hydraulic fracturing and infiltration of fluids into the damaged host rock an example from Dronning Maud Land, Antarctica. J Struct Geol 27:839–854

Engvik L, Stöckhert B, Engvik AK (2009) Fluid infiltration, heat transport, and healing of microcracks in the damage zone of magmatic veins: Numerical modeling. J Geophys Res 114: B05203. doi:10.1029/2008JB005880

Fraser G, McDougall I, Ellis DJ, Williams IS (2000) Timing and rate of isothermal decompression in Pan-African granulites from Rundvågshetta, East Antarctica. J Metamorph Geol 18:441–454

Grove M, Harrison TM (1996) $^{40}Ar^*$ diffusion in Fe-rich biotite. Am Mineral 81:940–951

Harley SL (2003) Archaean-Cambrian crustal development in East Antarctica: Metamorphic characteristics and tectonic implications. In: Yoshida M, Windley BF, Dasgupta S (eds) Proterozoic East Gondwana: Supercontinent Assembly and Breakup, Geological Society of London Special Publication 206, pp 203–230

Harrison TM (1981) Diffusion of ^{40}Ar in Hornblende. Contrib Mineral Petrol 78:324–331

Harrison TM, McDougall I (1982) The thermal significance of potassium feldspar K-Ar ages inferred from $^{40}Ar/^{39}Ar$ age spectrum results. Geochim Cosmochim Acta 46:1811–1820

Henjes-Kunst F (2004) Further evidence for Pan-African Polyphase magmatism and metamorphism in Central Dronning Maud Land, East Antarctica, from Rocks at Schirmakeroasise: a geochronological study. Geologishe Jahrbuch B96:255–292

Jacobs J, Thomas RJ (2004) Himalayan-type indenter-escape tectonics model for the southern part of the late Neoproterozoic-early Paleozoic East-African-Antarctic Orogen. Geology 32:721–724

Jacobs J, Ahrendt H, Kreutzer H, Weber K (1995) K-Ar, ^{40}Ar-^{39}Ar and apatite fission track evidence for Neoproterozoic and Mesozoic basement rejuvation in the Heimefrontfjella and Mannefallknausane (East Antarctica). Precambrian Res 75:251–262

Jacobs J, Fanning CM, Henjes-Kunst F, Olesch M, Paech H-J (1998) Continuation of the Mozambique Belt into East Antarctica: Grenville-Age metamorphism and Polyphase Pan-African High-Grade events in Central Dronning Maud Land. Journal of Geology 106:385–406

Jacobs J, Bauer W, Fanning CM (2003a) Late Neoproterozoic/Early Palaeozoic events in central Dronning Maud Land and significance for the southern extension of the East African Orogen into East Antarctica. Precambrian Res 126:27–53

Jacobs J, Klemb R, Fanning CM, Bauer W, Colombo F (2003b) Extensional collapse of the late Neoproterozoic-Early Paleozoic East African-Antarctic Orogen in central Dronning Maud Land, East Antarctica. In: Yoshida M, Windley BF, Dasgupta S (eds) Proterozoic East Gondwana: Supercontinent Assembly and Breakup, Geological Society London Special Publication 206, pp 271–288

Lee J-Y, Marti K, Severinghaus JP, Kawamura K, Yoo H-S, Lee JB, Kim JS (2006) A redetermination of the isotopic abundances of atmospheric Ar. Geochim Cosmochim Acta 70:4507–4512

Markl G, Henjes-Kunst F (2004) Magmatic conditions of formation and autometasomatism of post-kinematic charnockites in Central Dronning Maud Land, East Antarctica. Geologische Jahrbuch B96:139–188

McDougall I, Harrison TM (1999) Geochronology and thermochronology by the $^{40}Ar/^{39}Ar$ method. Oxford Monographs on Geology and Geophysics 9. Oxford University Press, New York

Meert JG (2003) A synopsis of events related to the assembly of eastern Gondwana. Tectonophysics 362:1–40

Meier S, Jacobs J, Olesch M (2004) Tectono-thermal evolution of Central Dronning Maud Land, East Antarctica, from Mid-Palaeozoic to Cenozoic times: zircon and apatite fission-track data from the Conradgebirge and Östliche Petermannkette. Geologische Jahrbuch B96:423–448

Mikhalsky EV, Beliatsky EV, Savva EV, Wetzel H-U, Federov LV, Weiser TH, Hahne K (1997) Reconnaissance Geochronologic Data on Polymetamorphic and Igneous Rocks of the Humboldt Mountains, Central Queen Maud Land, East Antarctica. In: Ricci CA (ed) Geological Evolution and Processes: The Antarctic Region. Terra Antarctica Publications, pp 45–53

Moyes AB (1993) The age and origin of the Jutulsessen granitic gneiss Gjelsvikfjella, Dronning Maud Land. S Afr J Antarct Res 23:25–32

Ohta Y, Tørudbakken BO, Shiraishi K (1990) Geology of Gjelsvikfjella and western Mülig-Hofmannfjella, Dronning Maud Land, East Antarctica. Polar Res 8:99–126

Paulsson O (2003) U-Pb geochronology of tectonothermal events related to the Rodinia and Gondwana supercontinents. Litholund theses- No 2 Published doctoral thesis, Lund University, Sweden

Paulsson O, Austrheim H (2003) A geochronological and geochemical study of rocks from the Gjelsvikfjella, Dronning Maud Land, Antarctica—implications for Mesoproterozoic correlations and assembly of Gondwana. Precambrian Res 125:113–138

Piazolo S, Markl G (1999) Humite- and scapolite-bearing assemblages in marble and calcsilicates of Dronning Maud Land, Antarctica: new data for Gondwana reconstructions. Journal of Metamorphic Geology 17:91–107

Pouchou JP, Pichoir F (1984) Cameca PAP program. Rech Aerospatiale 3:167–192

Renne PR, Mundil R, Balco G, Min K, Ludwig KR (2010) Joint determination of ^{40}K decay constants and $^{40}Ar^{*}/^{40}K$ for the Fish Canyon sanidine standard and improved accuracy for $^{40}Ar/^{39}Ar$ geochronology. Geochim Cosmochim Acta 74:5349–5367

Rex DC, Guise PG (1995) Evaluation of argon standards with special emphasis on time scale measurements. In: Odin GS (ed) Phanerozoic Time Scale. Bulletin Lias Information IUGS Subcommission on Geochronology 13, pp 21–23

Roland NW (2004) Pan-African granite-charnockite magmatism in Central Dronning Maud, Land East Antarctica: petrography geochemistry and plate tectonic implications. Geologische Jahrbuch B96:187–232

Stern RJ (1994) Arc assembly and continental collision in the Neoproterozoic East African Orogen: implications for the consolidation of Gondwanaland. Annu Rev Earth Planet Sci 22:319–351

Thost DE, Hensen B, Motoyoshi Y (1994) The geology of a rapidly uplifted medium and low pressure granulite facies terrane of Pan-African age: the Bolingen islands, Prydz Bay, Eastern Antarctica. Petrology 2:293–316

Villa IM (1998) Isotopic closure. Terra Nova 10:42–47

Villa IM, Puxeddu M (1994) Geochronology of the Larderello geothermal field: new data and the "closure temperature" issue. Contrib Mineral Petrol 115:415–426

Whitney DL, Evans BW (2010) Abbreviations of names of rock-forming minerals. Am Mineral 95:185–187

Zhao Y, Liu X, Wang S, Song B (1997) Syn- and post-tectonic cooling and exhumation in the Larsemann Hills, East Antarctica. Episodes 20:122–127